Hindawi Publishing Corporation
Journal of Applied Mathematics
Volume 2013, Article ID 583809, 11 pages
http://dx.doi.org/10.1155/2013/583809

Research Article

Mathematical Analysis of Casson Fluid Model for Blood Rheology in Stenosed Narrow Arteries

J. Venkatesan,[1] D. S. Sankar,[2] K. Hemalatha,[3] and Yazariah Yatim[4]

[1] *Department of Mathematics, Rajalakshmi Engineering College, Thandalam, Chennai 602 105, India*
[2] *Division of Mathematics, School of Advanced Sciences, VIT University, Chennai Campus, Chennai 600 127, India*
[3] *Department of Mathematics, Anna University, Chennai 600 025, India*
[4] *School of Mathematical Sciences, Universiti Sains Malaysia, 11800 Penang, Malaysia*

Correspondence should be addressed to D. S. Sankar; sankar_ds@yahoo.co.in

Received 1 April 2013; Accepted 14 July 2013

Academic Editor: Mohamed Fathy El-Amin

The flow of blood through a narrow artery with bell-shaped stenosis is investigated, treating blood as Casson fluid. Present results are compared with the results of the Herschel-Bulkley fluid model obtained by Misra and Shit (2006) for the same geometry. Resistance to flow and skin friction are normalized in two different ways such as (i) with respect to the same non-Newtonian fluid in a normal artery which gives the effect of a stenosis and (ii) with respect to the Newtonian fluid in the stenosed artery which spells out the non-Newtonian effects of the fluid. It is found that the resistance to flow and skin friction increase with the increase of maximum depth of the stenosis, but these flow quantities (when normalized with non-Newtonian fluid in normal artery) decrease with the increase of the yield stress, as obtained by Misra and Shit (2006). It is also noticed that the resistance to flow and skin friction increase (when normalized with Newtonian fluid in stenosed artery) with the increase of the yield stress.

1. Introduction

The study of the fluid dynamical aspects of blood flow through a stenosed artery is useful for the fundamental understanding of circulatory disorders. Stenosis in an artery is the narrowing of the blood flow area in the artery by the development of arteriosclerosis plaques due to the deposits of fats, cholesterol, and so forth on the inner wall of the artery. This leads to an increase in the resistance to flow and associated reduction in blood supply in the downstream which leads to serious cardiovascular diseases such as myocardial infarction and cerebral strokes [1–3].

Blood shows Newtonian fluid's character when it flows through larger diameter arteries at high shear rates, but it exhibits a remarkable non-Newtonian behavior when it flows through small diameter arteries at low shear rates [4, 5]. Moreover, there is an increase in viscosity of blood at low rate s of shear as the red blood cells tend to aggregate into the Rouleaux form [6]. Rouleaux form behaves as a semi-solid along the center forming a plug flow region. In the plug flow region, we have a flattened parabolic velocity profile rather than the parabolic velocity profile of a Newtonian fluid. This behavior can be modeled by the concept of yield stress. The yield stress for blood depends strongly on fibrinogen concentration and is also dependent on the hematocrit. The yield stress values for normal human blood is between 0.01 and 0.06 dyn/cm^2 [7].

Casson fluid model is a non-Newtonian fluid with yield stress which is widely used for modeling blood flow in narrow arteries. Many researchers have used the Casson fluid model for mathematical modeling of blood flow in narrow arteries at low shear rates. It has been demonstrated by Blair [8] and Copley [9] that the Casson fluid model is adequate for the representation of the simple shear behavior of blood in narrow arteries. Casson [10] examined the validity of Casson fluid model in his studies pertaining to the flow characteristics of blood and reported that at low shear rates the yield stress for blood is nonzero. It has been established by Merrill et al. [11] that the Casson fluid model predicts satisfactorily the flow behaviors of blood in tubes with the diameter of 130–1000 μm.

Charm and Kurland [12] pointed out in their experimental findings that the Casson fluid model could be the best representative of blood when it flows through narrow arteries at low shear rates and that it could be applied to human blood at a wide range of hematocrit and shear rates. Blair and Spanner [13] reported that blood behaves like a Casson fluid in the case of moderate shear rate flows, and it is appropriate to assume blood as a Casson fluid. Aroesty and Gross [14] have developed a Casson fluid theory for pulsatile blood flow through narrow uniform arteries. Chaturani and Samy [15] analyzed the pulsatile flow of Casson fluid through stenosed arteries using the perturbation method.

Herschel-Bulkley fluid is also a non-Newtonian fluid with yield stress which is more general in the sense that it contains two parameters such as the yield stress and power law index, whereas the Casson fluid has only one parameter which is the yield stress. Herschel-Bulkley fluid's constitutive equation can be reduced to the constitutive equations of Newtonian, Power law, and Bingham fluid models by taking appropriate values to the parameters. Chaturani and Ponnalagar Samy [16] analyzed the steady flow of Herschel-Bulkley fluid for blood flow through cosine-shaped stenosed arteries.

Misra and Shit [17] analyzed the steady flow of Herschel-Bulkley fluid for blood flow in narrow arteries with bell-shaped mild stenosis. The mathematical modeling of Casson fluid model for steady flow of blood in narrow arteries with bell-shaped mild stenosis was not studied by anyone so far, according to the knowledge of the authors. Hence, in the present study, a mathematical model is developed to analyze the blood flow at low shear rates in narrow arteries with mild bell-shaped stenosis, treating blood as Casson fluid model. The results of the present study are compared with the results of Misra and Shit [17], and Chaturani and Ponnalagar Samy [16] and some possible clinical applications to the present study are also given.

2. Formulation

Let us consider an axially symmetric, laminar, steady, and fully developed flow of a non-Newtonian incompressible viscous fluid (blood) in the axial direction (z) through a circular artery with bell-shaped mild stenosis. The non-Newtonian behavior of the flowing blood is characterized by Casson fluid model. The artery wall is assumed to be rigid (due to the presence of the stenosis) and the artery is assumed to be long enough so that the entrance and end effects can be neglected in the arterial segment under study. A cylindrical polar coordinate system (r, ψ, z) is used to analyze the blood flow, where r and z are the variables taken in the radial and axial directions, respectively, and ψ is the azimuthal angle. The geometry of the arterial segment with mild constriction is shown in Figure 1.

Since the blood flow in narrow arteries is slow, the magnitude of the inertial forces is negligibly small, and thus the inertial terms in the momentum equations are neglected. Since the considered flow is unidirectional and is in the axial direction, the radial component of the momentum equation

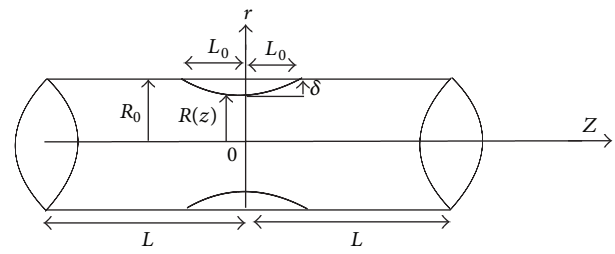

Figure 1: Geometry of the arterial segment with stenosis.

is ignored. The axial component of the momentum equation is simplified to the following:

$$-\frac{dp}{dz} = \frac{1}{r}\frac{d(r\tau)}{dr}, \tag{1}$$

where τ is the shear stress and p is the pressure. The constitutive equation (relationship between the shear stress and strain rate) of Casson fluid model is defined as follows:

$$-\frac{du}{dr} = f(\tau) = \begin{cases} \frac{1}{k}\left(\sqrt{\tau} - \sqrt{\tau_c}\right)^2, & \tau \geq \tau_c, \\ 0, & \tau \leq \tau_c, \end{cases} \tag{2}$$

where u is the velocity of blood in the axial direction, τ_c is the yield stress, and k is the viscosity coefficient of Casson fluid.

The geometry of the segment of the narrow artery with mild bell-shaped stenosis is mathematicaly defined as follows:

$$R(z) = R_0\left[1 - \frac{\delta}{R_0}e^{-m^2\epsilon^2 z^2/R_0^2}\right], \tag{3}$$

where R_0 is the radius of the normal artery, $R(z)$ is the radius of the artery in the stenosis region, δ is the depth of the stenosis at its throat, m is a parametric constant, and ϵ characterizes the relative length of the constriction, defined as $\epsilon = R_0/L_0$.

Equation (3) can be rewritten as

$$\frac{R(z)}{R_0} = 1 - ae^{-bz^2}, \tag{4}$$

where $a = \delta/R_0$ and $b = m^2\epsilon^2/R_0^2$. Note that a and b are the parameters in the nondimensional form corresponding to the maximum projection of the stenosis at its throat and variable length of the stenosis in the segment of the narrow artery under study, respectively. Equation (3) spells out that the bell-shaped geometry has the advantage of having two parameters such as a and b compared to cosine-curve shaped geometry which has only one parameter, namely, the maximum depth of the stenosis [15]. In the bell-shaped stenosis geometry, by keeping b as variable and a as constant, one can generate arteries with different stenosis lengths with the same maximum depth of the stenosis a, and also by keeping a as variable and b as constant one can generate arteries with different maximum depths with the same length of the stenosis. The different stenosis shapes obtained by varying the stenosis height a with 30% stenosis that is, $L_0 = 1.5$, are shown in

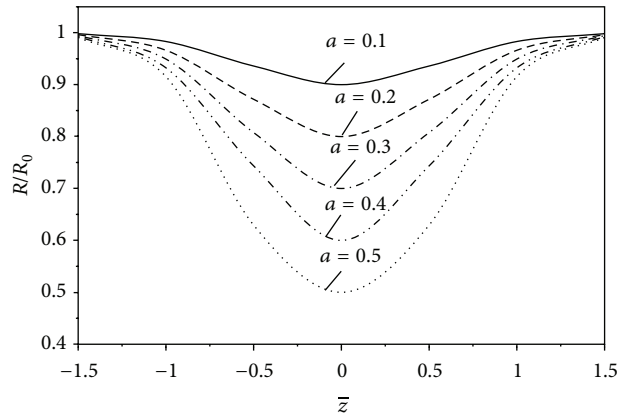

FIGURE 2: Stenosis geometries for different values of stenosis height a.

Figure 2. The percentage of stenosis is given by $L_0/L \times 100$. In the present study, we have taken $L = 5$ cm and $m = 2$ as taken by Misra and Shit [17].

Figure 3(a) depicts the shapes of stenoses with different lengths by fixing $a = 0.2$ and keeping b as variable (for different values of stenosis the length L_0 with fixed value of $m = 2$). Figure 3(b) shows the shapes of stenoses with different lengths by fixing $a = 0.2$ and varying the values of b (for different values of m and with a fixed value of $L_0 = 1.5$). It is noticed that the width of the stenosis decreases with the increase in the values of m.

Equations (1) and (2) have to be solved with the help of the following no slip boundary condition:

$$u = 0 \quad \text{at } r = R(z), \tag{5}$$

and the regularity condition

$$\tau \text{ is finite at } r = 0. \tag{6}$$

3. Method of Solution

Integrating (1) and then using (6), we get

$$\tau = -\frac{r}{2}\frac{dp}{dz}. \tag{7}$$

From (7), the skin friction τ_R is obtained as

$$\tau_R = -\frac{R}{2}\frac{dp}{dz}, \tag{8}$$

where $R = R(z)$.

The volumetric flow rate Q is as follows:

$$Q = \frac{\pi R^3}{\tau_R^3}\int_0^{\tau_R} \tau^2 f(\tau)\, d\tau, \tag{9}$$

where τ and τ_R are given by (7) and (8), respectively.

Substituting (2) into (9), we get

$$Q = \frac{\pi R^3}{\tau_R^3}\int_{\tau_C}^{\tau_R} \tau^2 \frac{1}{k}\left(\sqrt{\tau} - \sqrt{\tau_C}\right)^2 d\tau. \tag{10}$$

Integrating (10) and then simplifying, one can get

$$Q = \frac{\pi R^3}{4k}\tau_R\left\{1 - \frac{16}{7}\left(\frac{\tau_c}{\tau_R}\right)^{1/2} + \frac{4}{3}\left(\frac{\tau_c}{\tau_R}\right) - \frac{1}{21}\left(\frac{\tau_c}{\tau_R}\right)^4\right\}. \tag{11}$$

Since $\tau_c/\tau_R \ll 1$, neglecting the term involving $(\tau_c/\tau_R)^4$ in (11), we get the expression for flow rate as

$$Q = \frac{\pi R^3}{4k}\tau_R\left\{1 - \frac{16}{7}\left(\frac{\tau_c}{\tau_R}\right)^{1/2} + \frac{4}{3}\left(\frac{\tau_c}{\tau_R}\right)\right\}. \tag{12}$$

Using (8) in (12), we get

$$-\frac{dp}{dz} = \frac{128\tau_c}{49R} + \frac{8}{R}\left(\frac{Qk}{\pi R^3} - \frac{\tau_c}{147}\right) + \frac{64}{7R}\sqrt{\frac{kQ\tau_c}{\pi R^3} - \frac{\tau_c^2}{147}}. \tag{13}$$

Neglecting the term involving τ_c^2 in (13), we get

$$-\frac{dp}{dz} = \frac{128\tau_c}{49R} + \frac{8Qk}{\pi R^4} + \frac{64}{7R}\sqrt{\frac{kQ\tau_c}{\pi R^3}}. \tag{14}$$

Integrating (14) along the length of the artery and using the conditions that $p = p_1$ at $z = -L$ and $p = p_2$ at $z = L$, we obtain

$$\begin{aligned} p_1 - p_2 = {} & \frac{128\tau_c}{49R_0}\int_{-L}^{L}\frac{dz}{(R/R_0)} + \frac{8Qk}{\pi R_0^4}\int_{-L}^{L}\frac{dz}{(R/R_0)^4} \\ & + \frac{64}{7}\sqrt{\frac{Qk\tau_c}{\pi R_0^5}}\int_{-L}^{L}\frac{dz}{(R/R_0)^{5/2}}. \end{aligned} \tag{15}$$

Simplifying (15), one can obtain the following expression for pressure drop:

$$\begin{aligned} p_1 - p_2 = {} & \frac{256}{49}\frac{\tau_c}{R_0}\left\{(L - L_0) + \int_0^{L_0}\frac{dz}{(R/R_0)}\right\} \\ & + \frac{16Qk}{\pi R_0^4}\left\{(L - L_0) + \int_0^{L_0}\frac{dz}{(R/R_0)^4}\right\} \\ & + \frac{128}{7}\sqrt{\frac{Qk\tau_c}{\pi R_0^5}}\left\{(L - L_0) + \int_0^{L_0}\frac{dz}{(R/R_0)^{5/2}}\right\}. \end{aligned} \tag{16}$$

3.1. Resistance to Flow. The resistance to flow λ is defined as follows:

$$\lambda = \frac{p_1 - p_2}{Q}. \tag{17}$$

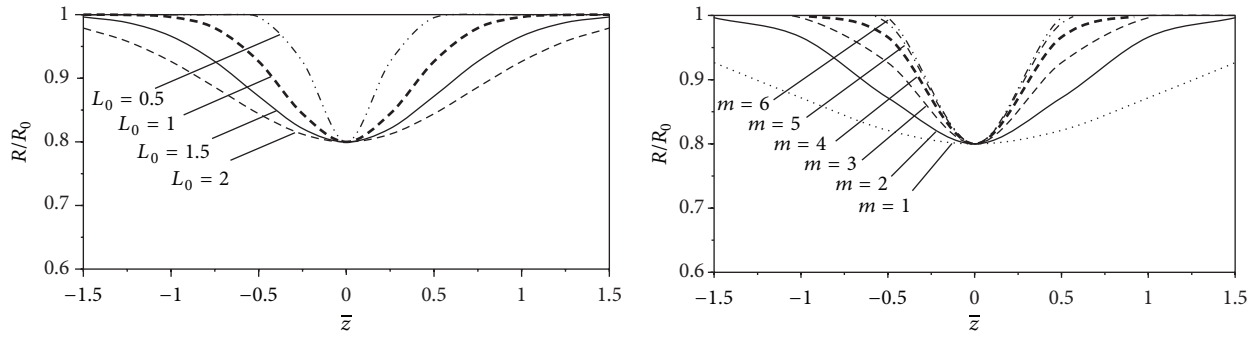

FIGURE 3: (a) Shapes of the arterial stenosis for different values of the stenosis length L_0. (b) Shapes of the arterial stenosis for different values of the stenosis shape parameter m.

The resistance to flow for Casson fluid in a stenosed artery is obtained as follows:

$$\lambda = \frac{256\tau_c}{49QR_0}\left\{(L-L_0)+\int_0^{L_0}\frac{dz}{(R/R_0)}\right\} + \frac{16k}{\pi R_0^4}\left\{(L-L_0)+\int_0^{L_0}\frac{dz}{(R/R_0)^4}\right\} + \frac{128}{7}\sqrt{\frac{k\tau_c}{\pi QR_0^5}}\left\{(L-L_0)+\int_0^{L_0}\frac{dz}{(R/R_0)^{5/2}}\right\}. \tag{18}$$

In the absence of any constriction ($\delta = 0$ and $R = R_0$), the resistance to flow (in the normal artery) λ_N is given by the following:

$$\lambda_N = \frac{16L}{R_0}\left\{\frac{k}{\pi R_0^3}+\frac{16\tau_c}{49Q}+\frac{8}{7}\sqrt{\frac{k\tau_c}{\pi QR_0^3}}\right\}. \tag{19}$$

The expression for resistance to flow in the dimensionless form is obtained as follows:

$$\overline{\lambda}_1 = \frac{\lambda}{\lambda_N} = 1-\frac{L_0}{L}+\frac{1}{L}\left(\frac{(16\tau_c/49Q)\,I_1+\left(k/\pi R_0^3\right)I_2+(8/7)\sqrt{(k\tau_c/\pi QR_0^3)}I_3}{(16\tau_c/49Q)+\left(k/\pi R_0^3\right)+(8/7)\sqrt{k\tau_c/\pi QR_0^3}}\right), \tag{20}$$

where $I_1 = \int_0^{L_0}(dz/(R/R_0))$, $I_2 = \int_0^{L_0}(dz/(R/R_0)^4)$, and $I_3 = \int_0^{L_0} dz/(R/R_0)^{(5/2)}$.

It is noted that $\overline{\lambda}_1$ measures the relative resistance in a stenosed artery compared to normal artery. Substituting the expression for R/R_0 from (4), the integrals I_1, I_2, and I_3 are reduced to the following:

$$I_1 = \int_0^{L_0}\frac{dz}{\left(1-ae^{-bz^2}\right)}, \qquad I_2 = \int_0^{L_0}\frac{dz}{\left(1-ae^{-bz^2}\right)^4}, \qquad I_3 = \int_0^{L_0}\frac{dz}{\left(1-ae^{-bz^2}\right)^{5/2}}. \tag{21}$$

Using a two-point Gauss quadrature formula, the integrals in (21) are evaluated as follows:

$$I_1 = \frac{L_0}{2}\left[\frac{1}{\left(1-ae^{-(bL_0^2/12)(4+2\sqrt{3})}\right)} + \frac{1}{\left(1-ae^{-(bL_0^2/12)(4-2\sqrt{3})}\right)}\right],$$

$$I_2 = \frac{L_0}{2}\left[\frac{1}{\left(1-ae^{-(bL_0^2/12)(4+2\sqrt{3})}\right)^4} + \frac{1}{\left(1-ae^{-(bL_0^2/12)(4-2\sqrt{3})}\right)^4}\right],$$

$$I_3 = \frac{L_0}{2}\left[\frac{1}{\left(1-ae^{-(bL_0^2/12)(4+2\sqrt{3})}\right)^{5/2}} + \frac{1}{\left(1-ae^{-(bL_0^2/12)(4-2\sqrt{3})}\right)^{5/2}}\right]. \tag{22}$$

If we want to compare the resistance to flow for different fluid models, we have to normalize it with respect to resistance to flow λ_{N_e} of Newtonian fluid in normal artery, and the respective expression for Casson fluid model is obtained as follows:

$$\begin{aligned}\overline{\lambda}_2 &= \frac{\lambda}{\lambda_{N_e}} \\ &= \left(1+\frac{16}{49}\left(\frac{\pi\tau_C R_0^3}{Qk}\right)+\frac{8}{7}\sqrt{\frac{\pi\tau_C R_0^3}{Qk}}\right) \\ &\quad\times\left(1-\frac{L_0}{L}\right)+\frac{1}{L}\left(\frac{16}{49}\left(\frac{\pi\tau_C R_0^3}{Qk}\right)I_1 \right. \\ &\quad\left. +I_2+\frac{8}{7}\sqrt{\frac{\pi\tau_C R_0^3}{Qk}}I_3\right),\end{aligned} \tag{23}$$

where

$$\lambda_{N_e} = \frac{16kL}{\pi R_0^4}, \tag{24}$$

which is obtained from (18) with $\delta = 0$, $R(z) = R_0$, and $\tau_c = 0$.

3.2. Skin Friction. From (8) and (14), the expression for the skin friction is obtained as follows:

$$\tau_R = -\frac{R}{2}\cdot\frac{dp}{dz} = \frac{64}{49}\tau_c + \frac{4Qk}{\pi R^3} + \frac{32}{7}\sqrt{\frac{kQ\tau_c}{\pi R^3}}. \tag{25}$$

In the absence of any constriction when ($R(z) = R_0$), the expression for the skin friction becomes the following:

$$\tau_N = \frac{64}{49}\tau_c + \frac{4Qk}{\pi R_0^3} + \frac{32}{7}\sqrt{\frac{kQ\tau_c}{\pi R_0^3}}. \tag{26}$$

The nondimensional form of skin friction with effects on stenosis is defined as the ratio between the skin friction in the stenosed artery and skin friction in the normal artery. From (25) and (26), the skin friction with effects on stenosis is obtained as

$$\overline{\tau}_1 = \frac{\tau_R}{\tau_N} = \frac{4Qk + (32/7)\left(Qk\tau_c\pi R_0^3\right)^{1/2}(R/R_0)^{3/2} + (64/49)\,\tau_c\pi R_0^3(R/R_0)^3}{(R/R_0)^3\left\{4Qk + (32/7)\left(Qk\tau_c\pi R_0^3\right)^{1/2} + (64/49)\,\tau_c\pi R_0^3\right\}}. \tag{27}$$

The nondimensional form of skin friction with effects on the non-Newtonian behavior of blood is defined as the ratio between the skin friction of the non-Newtonian fluid in the stenosed artery and the skin friction of the Newtonian fluid in the same stenosed artery. The expression for skin friction with effects on the non-Newtonian behavior of blood is obtained as follows:

$$\overline{\tau}_2 = \frac{\tau_R}{\tau_{N_e}} = \frac{1}{(R/R_0)^3} + \frac{16}{49}\left(\frac{\pi R_0^3\tau_C}{Qk}\right) + \frac{8}{7}\frac{1}{(R/R_0)^{3/2}}\sqrt{\frac{\pi R_0^3\tau_C}{Qk}}, \tag{28}$$

where

$$\tau_{N_e} = \frac{4kQ}{\pi R_0^3}. \tag{29}$$

4. Numerical Simulations of the Results

The objective of this study is to discuss the effects of various parameters on the physiologically important flow quantities such as skin friction, resistance to flow, and flow rate. The following parameters with their ranges mentioned as Q: 0–1, k: 2.0–7.0 $(\mathrm{CP})^n/\mathrm{sec}^{n-1}$, τ_c: 0.0–0.5 dyne/cm^2, $m = 2$, $L = 5$ cm, and $R_0 = 0.40$ are used to evaluate the expressions of these flow quantities and get data for plotting the graphs.

4.1. Skin-Friction

4.1.1. Effects of Stenosis on Skin-Friction. The variation of skin friction $\overline{\tau}_1$ with axial distance for different values of L_0/L and yield stress τ_c with $k = 4$ is shown in Figure 4. It is observed that the skin friction increases considerably with the increase in the stenosis length for a given value of yield stress τ_c, but it decreases very slightly when the yield stress increases for the fixed value of L_0/L. The same observations were recorded by Misra and Shit [17] for the Herschel-Bulkley fluid.

The variations of skin friction $\overline{\tau}_1$ at the midpoint of the stenosis with stenosis height δ/R_0 for different values of the yield stress τ_c with $k = 7$ and $L_0/L = 0.3$ are sketched in Figure 5. It is noted that the skin friction decreases marginally as the yield stress increases.

The estimates of skin friction $\overline{\tau}_1$ for different values of axial variable z and viscosity coefficient k with $\tau_c = 0.05$ and

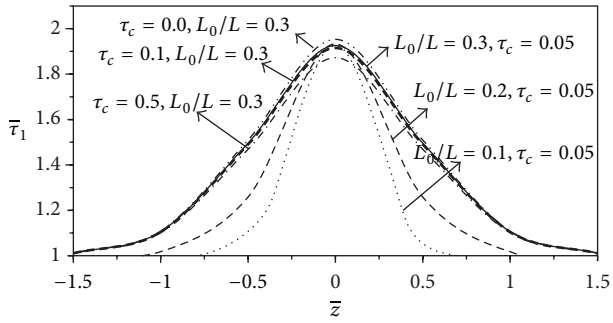

Figure 4: Variations of skin friction $\overline{\tau}_1$ with axial distance for different percentages of stenosis L_0/L and yield stress τ_c.

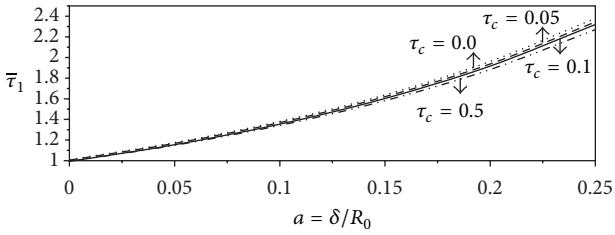

Figure 5: Variations of skin friction $\overline{\tau}_1$ with stenosis height a for different values of yield stress τ_c.

30% stenosis are computed in Table 1. It is observed that the skin friction increases very slightly with the increase of the viscosity coefficient.

In order to compare our results with those of Misra and Shit [17], the variations of skin friction $\overline{\tau}_1$ with axial distance for different fluids are shown in Figure 6 for 30% of stenosis with $k = 4$ and $\tau_c = 0.05$. It is observed that the plot of the skin friction of Casson fluid model lies between those of the Herschel-Bulkley fluid model with $n = 1$ and $n = 1.05$. Here, the skin friction is normalized with respect to the normal artery with the same fluid, as was done by Misra and Shit [17].

The mathematical form of cosine curve-shaped geometry for stenosis given by Chaturani and Ponnalagar Samy [16] is reproduced as follows:

$$\frac{R(z)}{R_0} = 1 - \frac{\delta}{2R_0}\left[1 + \cos\frac{2\pi}{L_0}\left(z - d - \frac{L_0}{2}\right)\right], \quad d \le z \le d + L_0. \tag{30}$$

For computation, values of the parameters are taken as $L = 10$, $d = 3.5$, and $L_0 = 3$.

The variations of skin friction $\overline{\tau}_1$ with axial distance for Casson fluid model with cosine- and bell-shaped stenosis geometries with 30% stenosis and with $k = 4$ and $\tau_c = 0.05$ are shown in Figure 7 (the data for plotting the graph is computed from (27)). It is found that the skin friction in cosine curve-shaped stenosed arteries is considerably higher than that in bell-shaped stenosed arteries.

4.1.2. Effects of Non-Newtonian Behavior on Skin-Friction. We can study the effects of different non-Newtonian fluids if we normalize it with respect to Newtonian fluid as done by [15, 16, 18–20]. In this case, the following results are in agreement with the results given by these authors but are opposite in nature to those given in Section 4.1.1 except for the variations of skin friction with axial distance for different values of stenosis length as given in Figure 8.

Table 1: Variations of the skin friction $\overline{\tau}_1$ with axial distance for different values of viscosity with $\tau_c = 0.05$ and $L_0/L = 0.3$.

z	$\overline{\tau}$		
	$k = 2$	$k = 4$	$k = 7$
−1.5	1.01069	1.010799	1.010864
−1	1.104858	1.105946	1.106599
−0.5	1.490229	1.495693	1.49897
0	1.915269	1.926048	1.932516
0.5	1.490229	1.495693	1.49897
1	1.104858	1.105946	1.106599
1.5	1.01069	1.010799	1.010864

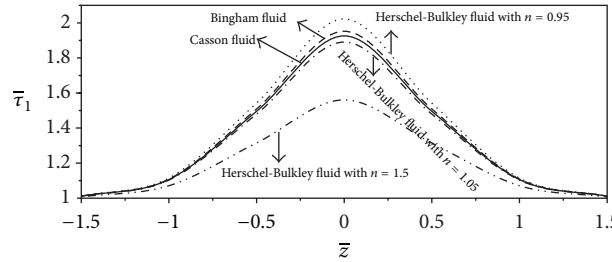

Figure 6: Variations of skin friction $\overline{\tau}_1$ with axial distance for different fluids.

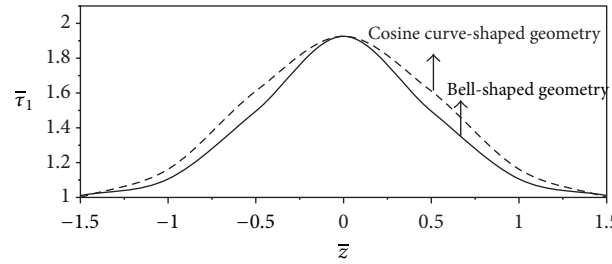

Figure 7: Variations of skin friction $\overline{\tau}_1$ for Casson fluid with axial distance for different arterial geometries.

The variations of skin friction $\overline{\tau}_2$ with axial distance for different values of L_0/L and for a given $k = 4$ and $\tau_c = 0.05$ are illustrated in Figure 9. It is observed that the skin friction increases considerably with the increase in the stenosis length.

Figure 10 sketches the variations of skin friction $\overline{\tau}_2$ with axial distance for different values of yield stress with $k = 4$ and $L_0/L = 0.3$. It is observed that the skin friction increases marginally with the increase in the yield stress τ_c of the fluid.

The variations of skin friction $\overline{\tau}_2$ at the midpoint of the stenosis with stenosis height δ/R_0 for different values of the yield stress τ_c with $k = 4$ and $L_0/L = 0.3$ are shown in

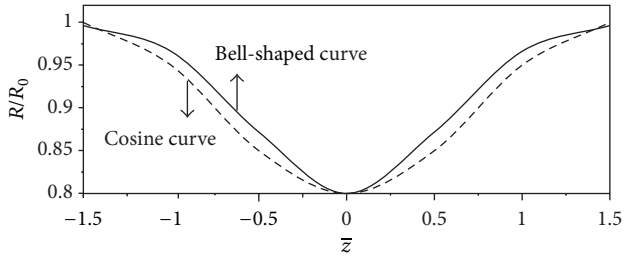

Figure 8: Comparison of cosine- and bell-shaped stenosis shapes.

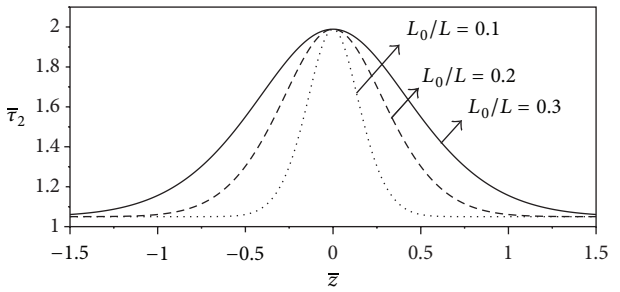

Figure 9: Variations of skin friction $\overline{\tau}_2$ with axial distance for different values of stenosis size L_0/L.

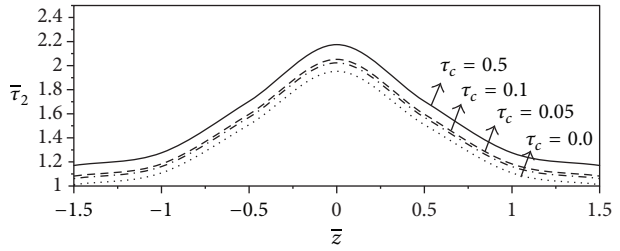

Figure 10: Variations of skin friction $\overline{\tau}_2$ with axial distance for different values of yield stress τ_C.

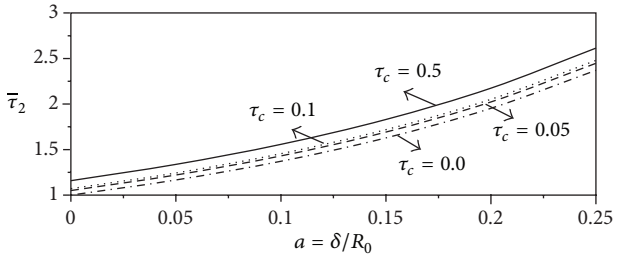

Figure 11: Variations of skin friction $\overline{\tau}_2$ with stenosis height δ/R_0 for different values of yield stress τ_C.

Figure 11. It is clear that the skin friction increases marginally when the yield stress increases.

Figure 12 depicts the variations of skin friction $\overline{\tau}_2$ with axial distance for different values of viscosity coefficient k for $\tau_c = 0.05$ and 30% of stenosis. One can notice that the skin friction decreases slightly as viscosity increases.

Figure 13 shows the variations of skin friction $\overline{\tau}_2$ with axial distance for different fluid models using cosine-shaped stenosis with 30% of stenosis, yield stress $\tau_c = 0.05$, and $k = 4$. It is observed that the skin friction of Casson fluid model lies between those of the Herschel-Bulkley fluid model with $n = 0.95$ and $n = 1$.

The variations of skin friction $\overline{\tau}_2$ with axial distance for different fluid models using bell-shaped stenosis with 30% of stenosis, yield stress $\tau_c = 0.05$, and $k = 4$ are shown in Figure 14. It is observed that the skin friction of Casson fluid model lies between those of the Herschel-Bulkley fluid model with $n = 0.95$ and $n = 1$.

Figure 15 shows the variations of skin friction $\overline{\tau}_2$ with axial distance for Casson fluid model with cosine- and bell-shaped geometries with 30% stenosis, $k = 4$, and $\tau_c = 0.05$ (data computed using (28)). It is seen that the cosine-shaped stenosis has a greater width than that of bell-shaped stenosis as depicted in Figure 8.

Misra and Shit [17] have analyzed the variations of skin friction with axial distance for different values of power law index and yield stress and reported that the skin friction decreases with increase in yield stress. If normalized with Newtonian fluid, the skin friction increases considerably when the yield stress increases with axial distance for 30% stenosis, $k = 4$ as displayed in Figure 16.

4.2. Resistance to Flow. The variations of resistance to flow $\overline{\lambda}_1$ with the height of the stenosis δ/R_0 for different values of stenosis length L_0/L with viscosity coefficient $k = 4$ and yield stress $\tau_c = 0.05$ are shown in Figure 17. It is found that the flow resistance increases nonlinearly with the increase in the stenosis size.

Using the result (23), the variations of resistance to flow $\overline{\lambda}_2$ with stenosis height for different values of stenosis length, for the given $k = 4$ and $\tau_C = 0.05$ are shown in Figure 18. It is observed that the flow resistance decreases considerably when the length of the stenosis increases. Also, the variations of resistance to flow $\overline{\lambda}_2$ with stenosis height for different values of yield stress and for $k = 4$ and $L_0/L = 0.3$ is shown in Figure 19. It is clear that the resistance to flow increases significantly with the increase in the yield stress.

4.3. Flow Rate. Figure 20 depicts the variation of flow rate with axial distance for different values of viscosity coefficient k and yield stress τ_c with 30% of stenosis. One can notice that the flow rate decreases significantly with the increase of either the viscosity coefficient or the yield stress. It is also observed that the flow rate decreases very significantly (nonlinearly) at the throat of the stenosis for lower values of either the yield stress or viscosity coefficient and slowly (almost linearly) for higher values of either the yield stress or viscosity coefficient.

4.4. Physiological Application. To highlight some possible clinical applications of the present study, the data used by Sankar [21] (the radii of different arteries and flow rate) are used to compute the physiologically important flow quantities such as resistance to flow and skin friction. The values of the parameters are taken as $k = 3.5$ and $\tau_c = 0.04$. The dimensionless resistance to flow $\overline{\lambda}_2$ and skin friction $\overline{\tau}_2$ are

Table 2: Estimates of resistance to flow $\overline{\lambda}_2$ and skin friction (dimensionless) $\overline{\tau}_2$ in arteries with different radii with $L_0/L = 1$.

Blood vessels Radius R_0 (cm) Flow rate Q (cm^3 s^{-1})	τ_c'	$a = 0.10$		$a = 0.15$	
		$\overline{\lambda}$	$\overline{\tau}$	$\overline{\lambda}$	$\overline{\tau}$
Aorta (1, 71.67)	1.529080×10^{-2}	1.567142	1.722748	1.745439	2.008973
Femoral (0.5, 19.63)	5.718029×10^{-3}	1.429659	1.581644	1.598551	1.856356
Carotid (0.4, 12.57)	4.571948×10^{-3}	1.407374	1.558726	1.574716	1.831521
Coronary (0.15, 3.47)	8.733753×10^{-4}	1.303768	1.451998	1.463802	1.715671
Arteriole (0.008, 0.00008)	5.629388×10^{-3}	1.428014	1.579953	1.596792	1.854524

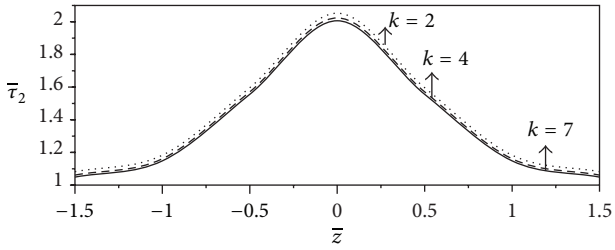

Figure 12: Variations of skin friction $\overline{\tau}_2$ with axial distance for different values of viscosity k.

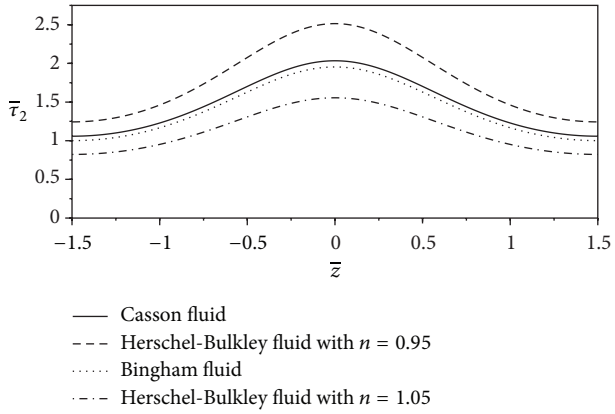

Figure 13: Variations of skin friction $\overline{\tau}_2$ with axial distance for different fluid models with cosine-shaped stenosis.

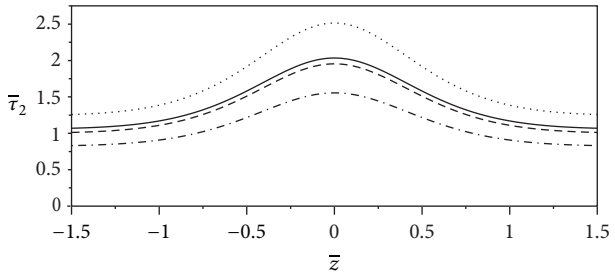

Figure 14: Variations of skin friction $\overline{\tau}_2$ with axial distance for different fluid models with bell-shaped stenosis.

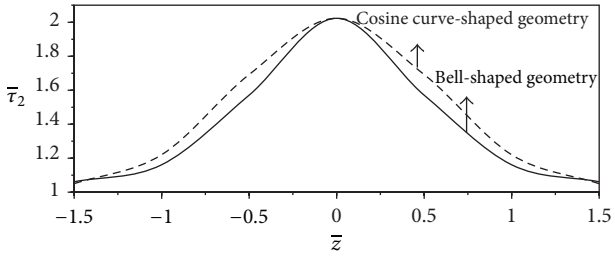

Figure 15: Variations of skin friction $\overline{\tau}_2$ of Casson fluid model with axial distance for different geometries.

computed for arteries with different radii and with $m = 2$ and $L_0/L = 1$ from (23) and (28) (normalized with Newtonian fluid in stenosed artery) and are presented in Table 2. It is noted that the resistance to flow increases, considerably when the stenosis height increases and skin friction significantly increases with the increase of stenosis height.

The percentages of increase in resistance to flow and skin friction over that for uniform diameter tube (no stenosis) and for arteries with different radii are computed in Table 3. One can observe that the percentages of increase in resistance to flow and skin friction increase significantly when stenosis height increases. Comparisons of resistance to flow ($\overline{\lambda}_2$) in bell-shaped stenosed arteries and cosine curve-shaped stenosed arteries with different values of stenosis size parameters a, L_0, and m are given in Table 4. It is recorded that the resistance to flow in bell-shaped stenosed artery increases considerably when the length of the stenosis increases, and also it significantly increases when stenosis height increases. But it marginally decreases with the increase of the stenosis length parameter m. It is also found that for

Table 3: Estimates of the percentage of increase in resistance to flow $\overline{\lambda}_2$ and skin friction $\overline{\tau}_2$ for arteries with different radii with $L_0/L = 1$ and $\tau_c = 0.04$ dyn cm^{-2}.

Blood vessels	τ_c'	$a = 0.10$		$a = 0.15$	
		$\overline{\lambda}$ (%)	$\overline{\tau}$ (%)	$\overline{\lambda}$ (%)	$\overline{\tau}$ (%)
Aorta	1.529080×10^{-2}	20.31	32.25	34.00	54.23
Femoral	5.718029×10^{-3}	21.13	34.00	35.44	57.28
Carotid	4.571948×10^{-3}	21.27	34.31	35.69	57.82
Coronary	8.733753×10^{-4}	22.00	35.86	36.97	60.53
Arteriole	5.629388×10^{-3}	21.14	34.03	35.45	57.32

Table 4: Estimates of percentage of increase in resistance to flow $\overline{\lambda}_2$ for arteries with different radii and with (i) bell-shaped stenosis (ii) cosine curve-shaped stenosis.

Blood vessels	Bell-shaped stenosis $\overline{\lambda}_2$ (%)					Cosine curve-shaped stenosis $\overline{\lambda}_2$ (%)	
	$a = 0.1$ $m = 2$ $L_0 = 1.0$	$a = 0.1$ $m = 2$ $L_0 = 1.5$	$a = 0.1$ $m = 3$ $L_0 = 1.5$	$a = 0.2$ $m = 3$ $L_0 = 1.5$	$a = 0.2$ $m = 2$ $L_0 = 1.5$	$a = 0.1$ $L_0 = 1.0$	$a = 0.2$ $L_0 = 1.5$
Aorta	4.06	6.09	4.33	10.42	15.31	4.28	15.79
Femoral	4.23	6.34	4.50	10.87	15.99	4.45	16.78
Carotid	4.25	6.38	4.53	10.95	16.11	4.50	16.96
Coronary	4.40	6.60	4.68	11.35	16.72	4.71	17.86
Arteriole	4.23	6.34	4.50	10.88	16.00	4.47	16.79

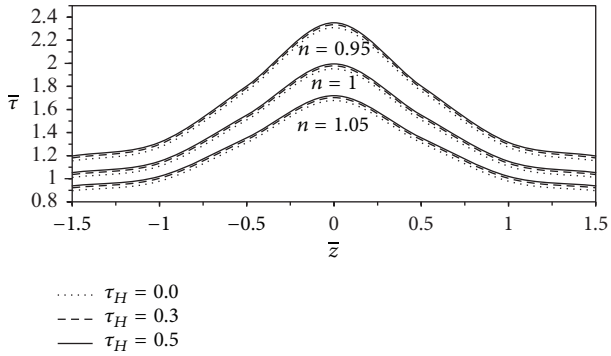

Figure 16: Variations of skin friction with axial distance for different values of power index and yield stress τ_H.

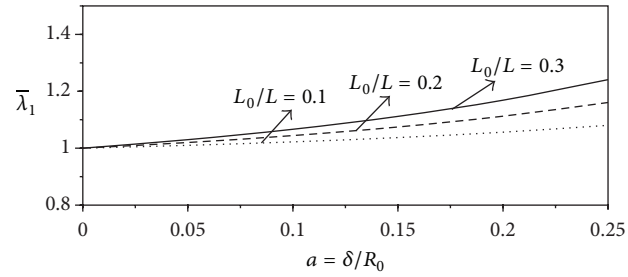

Figure 17: Variations of flow resistance $\overline{\lambda}_1$ with stenosis height δ/R_0 for different values of stenosis length L_0/L.

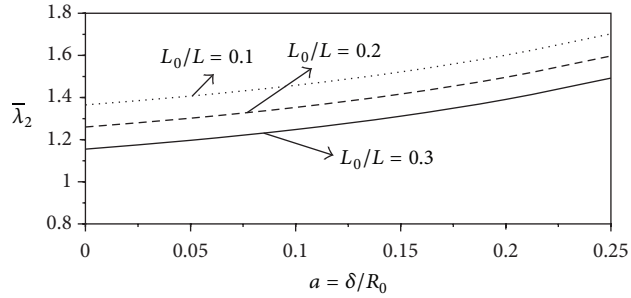

Figure 18: Variations of flow resistance $\overline{\lambda}_2$ with stenosis height δ/R_0 for different values of stenosis length L_0/L.

a given set of values of the parameters, the percentage of increase in resistance to flow in the case of bell-shaped stenosed artery is slightly lower than that of cosine curve-shaped stenosed artery. This is physically verified with the depth of the stenosis for cosine-shaped stenosis (shown in Figure 8) being more; the resistance to flow is higher in this type of stenosis geometry compared to the bell-shaped stenosis geometry.

5. Conclusion

The present study analyzed the steady flow of blood in a narrow artery with bell-shaped mild stenosis, treating blood as Casson fluid, and the results are compared with the results of Misra and Shit for, Herschel-Bulkley fluid model [17] and also with the results of Chaturani and Ponnalagar Samy [16] (for blood flow in cosine curve-shaped stenosed arteries, treating blood as Herschel-Bulkley fluid model). The main findings of the present mathematical analysis are as follows:

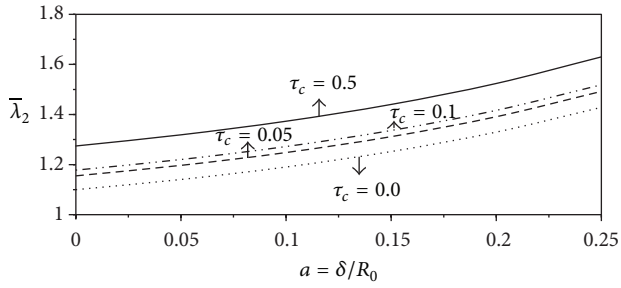

FIGURE 19: Variations of flow resistance $\overline{\lambda}_2$ with stenosis height δ/R_0 for different values of yield stress τ_c.

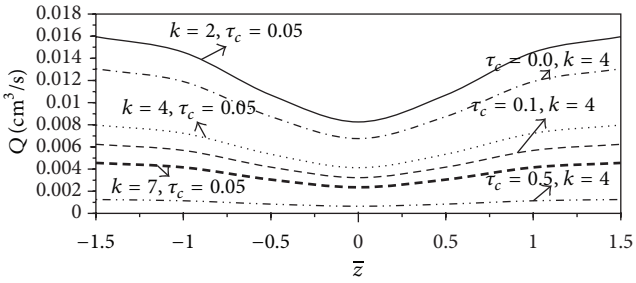

FIGURE 20: Variations of the rate of flow with axial distance for different values of viscosity k and yield stress τ_c.

(i) Whether normalized with respect to non-Newtonian or Newtonian fluid in normal artery (i.e., in both cases of the effect of stenosis and the effect of non-Newtonian fluid) we notice the following.

(1) Skin friction increases with the increase of depth and length of the stenosis.

(2) Skin friction of Casson fluid model is significantly lower than that of the Herschel-Bulkley fluid model.

(3) Skin friction in bell-shaped stenosed artery is considerably lower than that in the cosine curve-shaped stenosed artery.

(ii) The effect of stenosis on blood flow is that the resistance to flow increases when either the stenosis length or depth increases.

(iii) The effect of non-Newtonian fluid on blood flow is that the resistance to flow increases significantly with the increase of yield stress, but it decreases when either the stenosis length or depth increases.

(iv) The percentage of increase in resistance to flow in the case of bell-shaped stenosed artery is slightly lower than that of the cosine curve-shaped stenosed artery in the case of normalization with respect to Newtonian fluid.

(v) Flow rate decreases with the increase of the yield stress and viscosity coefficient.

Hence, in view of the results obtained, we conclude that the present study may be considered as an improvement in the studies of the mathematical modeling of blood flow in narrow arteries with mild stenosis.

Nomenclature

τ: Shear stress
τ_c: Yield stress for Casson fluid
τ_R: Skin friction in stenosed artery
$\overline{\tau}_1$: Nondimensional skin friction normalized with non-Newtonian fluid
$\overline{\tau}_2$: Nondimensional skin friction normalized with Newtonian fluid
τ_N: Skin friction in normal artery normalized with non-Newtonian fluid
τ_{N_e}: Skin friction in normal artery normalized with Newtonian fluid
δ: Stenosis height
λ: Flow resistance
$\overline{\lambda}_1$: Nondimensional flow resistance normalized with non-Newtonian fluid
$\overline{\lambda}_2$: Nondimensional flow resistance normalized with Newtonian fluid
$\overline{\lambda}_N$: Flow resistance in normal artery normalized with non-Newtonian fluid
$\overline{\lambda}_{N_e}$: Flow resistance in normal artery normalized with Newtonian fluid
Q: Volumetric flow rate
r: Radial coordinate
z: Axial coordinate
u: Radial velocity
R_0: Radius of the normal artery
$R(z)$: Radius of the artery in the stenosed portion
L: Half-length of segment of the narrow artery
L_0: Half-length of the stenosis
p: Pressure
k: Viscosity coefficient.

Acknowledgments

The authors thank S. V. Subhashini, Assistant Professor (SG), Department of Mathematics, Anna University, Chennai, for her useful suggestions and timely help for improving the quality of the paper. The research work is supported by the Research University grant of the Universiti Sains Malaysia, Malaysia. RU Grant no. 1001/PMATHS/811177.

References

[1] M. E. Clark, J. M. Robertson, and L. C. Cheng, "Stenosis severity effects for unbalanced simple-pulsatile bifurcation flow," *Journal of Biomechanics*, vol. 16, no. 11, pp. 895–906, 1983.

[2] D. Liepsch, M. Singh, and M. Lee, "Experimental analysis of the influence of stenotic geometry on steady flow," *Biorheology*, vol. 29, no. 4, pp. 419–431, 1992.

[3] S. Cavalcanti, "Hemodynamics of an artery with mild stenosis," *Journal of Biomechanics*, vol. 28, no. 4, pp. 387–399, 1995.

[4] V. P. Rathod and S. Tanveer, "Pulsatile flow of couple stress fluid through a porous medium with periodic body acceleration and

magnetic field," *Bulletin of the Malaysian Mathematical Sciences Society*, vol. 32, no. 2, pp. 245–259, 2009.

[5] G. R. Cokelet, "The rheology of human blood," in *Biomechanics*, Y. C. Fung et al., Ed., p. 63, Prentice-hall, Englewood Cliffs, NJ, USA, 1972.

[6] W. Boyd, *Text Book of Pathology: Structure and Functions in Diseases*, Lea and Febiger, Philadelphia, Pa, USA, 1963.

[7] B. C. Krishnan, S. E. Rittgers, and A. P. Yoganathan, *Biouid Mechanics: The Human Circulation*, Taylor and Francis, New York, NY, USA, 2012.

[8] G. W. S. Blair, "An equation for the flow of blood, plasma and serum through glass capillaries," *Nature*, vol. 183, no. 4661, pp. 613–614, 1959.

[9] A. L. Copley, "Apparent viscosity and wall adherence of blood systems," in *Flow Properties of Blood and Other Biological Systems*, A. L. Copley and G. Stainsly, Eds., Pergamon Press, Oxford, UK, 1960.

[10] N. Casson, "Rheology of disperse systems," in *Flow Equation for Pigment Oil Suspensions of the Printing Ink Type. Rheology of Disperse Systems*, C. C. Mill, Ed., pp. 84–102, Pergamon Press, London, UK, 1959.

[11] E. W. Merrill, A. M. Benis, E. R. Gilliland, T. K. Sherwood, and E. W. Salzman, "Pressure-flow relations of human blood in hollow fibers at low flow rates," *Journal of Applied Physiology*, vol. 20, no. 5, pp. 954–967, 1965.

[12] S. Charm and G. Kurland, "Viscometry of human blood for shear rates of 0-100,000 sec^{-1}," *Nature*, vol. 206, no. 4984, pp. 617–618, 1965.

[13] G. W. S. Blair and D. C. Spanner, *An Introduction to Biorheology*, Elsevier Scientific, Oxford, UK, 1974.

[14] J. Aroesty and J. F. Gross, "Pulsatile flow in small blood vessels. I. Casson theory," *Biorheology*, vol. 9, no. 1, pp. 33–43, 1972.

[15] P. Chaturani and R. P. Samy, "Pulsatile flow of Casson's fluid through stenosed arteries with applications to blood flow," *Biorheology*, vol. 23, no. 5, pp. 499–511, 1986.

[16] P. Chaturani and V. R. Ponnalagar Samy, "A study of non-Newtonian aspects of blood flow through stenosed arteries and its applications in arterial diseases," *Biorheology*, vol. 22, no. 6, pp. 521–531, 1985.

[17] J. C. Misra and G. C. Shit, "Blood flow through arteries in a pathological state: a theoretical study," *International Journal of Engineering Science*, vol. 44, no. 10, pp. 662–671, 2006.

[18] D. S. Sankar, "Two-fluid nonlinear mathematical model for pulsatile blood flow through stenosed arteries," *Bulletin of the Malaysian Mathematical Sciences Society*, vol. 35, no. 2A, pp. 487–498, 2012.

[19] D. S. Sankar and K. Hemalatha, "Pulsatile flow of Herschel-Bulkley fluid through stenosed arteries—a mathematical model," *International Journal of Non-Linear Mechanics*, vol. 41, no. 8, pp. 979–990, 2006.

[20] S. U. Siddiqui, N. K. Verma, and R. S. Gupta, "A mathematical model for pulsatile flow of Herschel-Bulkley fluid through stenosed arteries," *Journal of Electronic Science and Technology*, vol. 4, pp. 49–466, 2010.

[21] D. S. Sankar, "Perturbation analysis for blood flow in stenosed arteries under body acceleration," *International Journal of Nonlinear Sciences and Numerical Simulation*, vol. 11, no. 8, pp. 631–653, 2010.